

# PhISH-Net: Physics Inspired System for High Resolution Underwater Image Enhancement

Aditya Chandrasekar, Manogna Sreenivas, Soma Biswas

Indian Institute of Science, Bangalore

{caditya, manognas, somabiswas}@iisc.ac.in

## Abstract

*Underwater imaging presents numerous challenges due to refraction, light absorption, and scattering, resulting in color degradation, low contrast, and blurriness. Enhancing underwater images is crucial for high-level computer vision tasks, but existing methods either neglect the physics-based image formation process or require expensive computations. In this paper, we propose an effective framework that combines a physics-based Underwater Image Formation Model (UIFM) with a deep image enhancement approach based on the retinex model. Firstly, we remove backscatter by estimating attenuation coefficients using depth information. Then, we employ a retinex model-based deep image enhancement module to enhance the images. To ensure adherence to the UIFM, we introduce a novel Wideband Attenuation prior. The proposed PhISH-Net framework achieves real-time processing of high-resolution underwater images using a lightweight neural network and a bilateral-grid-based upsample. Extensive experiments on two underwater image datasets demonstrate the superior performance of our method compared to state-of-the-art techniques. Additionally, qualitative evaluation on a cross-dataset scenario confirms its generalization capability. Our contributions lie in combining the physics-based UIFM with deep image enhancement methods, introducing the wideband attenuation prior, and achieving superior performance and efficiency.*

## 1. Introduction

Underwater imaging is important for various applications such as marine life studies, coral reef monitoring, ocean exploration, and underwater robotics [35]. However, capturing high-quality underwater images is challenging due to factors like refraction, selective light absorption, and scattering. Colors are attenuated differently underwater, with shorter wavelength colors (green and blue) appearing more pronounced due to scattering and longer wavelength colors (red and orange) being absorbed. This effect

is amplified at greater depths, resulting in color degradation, low contrast, and blurriness in underwater images. These challenges make it difficult for computer vision tasks like segmentation, object detection, and tracking. To address this, we propose an effective framework that combines deep image enhancement techniques with a physics-based image model that considers light scattering in water.

Early works [1, 28] perform Underwater Image Enhancement (UIE) by correcting contrast, brightness, saturation etc. However, unlike images captured in the air, it is crucial to consider the physical process of underwater image formation when processing these images. Another line of works [2, 3, 52] use Underwater Image Formation Models (UIFM) to improve the visual clarity of underwater images. These models mathematically simulate how light interacts with the underwater environment and how imaging devices capture the images. UIFM-based underwater image enhancement methods often estimate unknown color and light scattering attenuation coefficients to recover clean image signals based on the mathematical model. However, these methods are computationally expensive for real-time applications as they require estimating attenuation coefficients for each image. Recent studies [17, 20, 43] have been inspired by the success of deep neural networks in tasks like image dehazing and low-light image enhancement, and have applied deep networks for underwater image enhancement. These approaches learn the mapping between degraded images and their enhanced counterparts. Additionally, most underwater image datasets consist of high-resolution images [10, 40], but these models often process them at lower resolutions, limiting their performance.

In this work, we propose an effective framework that leverages the formulation of physics based UIFM with retinex model based deep image enhancement framework. We employ the well established UIFM model proposed in Sea-Thru [4], where an underwater image is modeled to have two components (i) *Direct signal* representing the primary source of image formation and contains the true characteristics of the subject being captured, however with attenuated colors as a function of distance and wavelength;



Figure 1. Sample results for images from the UIEB dataset. **Top:** input; **Bottom:** corresponding enhanced image.

(ii) *Backscatter signal* arising from light scattering by particles suspended in the water. Backscatter tends to be more prominent in underwater imaging due to the higher concentration of suspended particles compared to the air.

Firstly, we propose to estimate and remove backscatter by estimating the attenuation coefficients as proposed in [4]. However, this step requires depth information, which is not available for most underwater image datasets as it is difficult to obtain. To circumvent this, we propose the utilization of an off-the-shelf monocular depth estimation method [48], which we found to be effective. On observing that these backscatter-removed images resemble low-light underexposed images, we propose to use a retinex model-based deep image enhancement module to perform UIE.

Physical model based methods estimate attenuation coefficients for each image individually, while data driven methods ignore the physical image formation process and treat UIE as low light image enhancement problem. In this context, we aim to leverage the effectiveness of both lines of work by proposing a novel *Wideband Attenuation* prior. Through this, while performing image enhancement with PhISH-Net, we ensure that it also adheres to the UIFM model [4], thus considering the characteristics of light scattering in water. We perform most of the computation on low-resolution images and subsequently employ a bilateral grid-based upsampling module to generate the high-resolution enhanced images.

Our study encompasses comprehensive experiments on two underwater image datasets: UIEB [40] and EUVP [35]. In addition, we qualitatively evaluate the cross-dataset performance by testing the model trained on EUVP on another dataset named SQUID [10]. Our method consistently outperforms state-of-the-art (SOTA) UIE methods. Furthermore, the proposed PhISH-Net framework is computationally efficient and lightweight with 0.55M parameters. The key contributions of our work are as follows:

- The proposed PhISH-Net framework combines the physics-based UIFM with a deep image enhancement approach based on the retinex model.

- We propose a novel wideband attenuation prior conditioned on the UIFM while learning PhISH-Net. This takes into account the optical characteristics and color attenuation properties of water.
- Our approach exhibits superior performance compared to SOTA on two underwater image datasets. Further, we demonstrate its effectiveness by qualitatively evaluating its cross-dataset generalization performance.

## 2. Related Work

In this section, we provide a comprehensive review of the latest advancements in UIE.

**Image Processing based Methods** aim to restore the clarity of underwater images by modifying their appearance based on prior visual characteristics. They employ various image processing techniques, such as contrast adjustment [34], histogram equalization (HE) [49], white balance [47], and fusion-based approaches [7, 8]. Hassan *et al.* [32] propose to use contrast limited adaptive HE as a pre-processing step for further retinex based enhancement.

**Physical Model based Methods** extend the principles of prior model-based dehazing algorithms to underwater scenes, treating UIE as an inversion problem. The objective is to restore the image by effectively reversing the degradation caused by the underwater imaging process. Various approaches have been developed based on different priors, such as the dark channel prior [13–15, 53, 58], red channel prior [24], attenuation curve prior [66], backscatter pixel prior [75] and minimum information prior [42]. Notable model-based methods include works by Akkaynak *et al.* [3], Berman *et al.* [10], Pei *et al.* [52], Xie *et al.* [68], HLRP [76], MLLE [74], and ICSP [33].

**Data Driven Methods** with deep learning have recently gained prominence in UIE. CNN based methods include WaterNet [40], UWCNN [38], SGUIE-Net [56], UICoE-

Net [57] and UIE-Net [64]. GAN based approaches include UGAN [19], UW-GAN [60], Spiral-GAN [31], FunIE-GAN [35], WaterGAN [44], Dense GAN [27], FE-GAN [29], TOPAL [36], and CycleGAN [41]. However, such methods perform poorly on real-world images due to their reliance on large synthetic datasets for training as they fail to take into account the domain shift problem between synthetic and real-world data [67]. They also disregard the physical process of image formation under water.

**Low Light Image Enhancement** Given the dimly lit nature of the backscatter removed images, UIE can benefit from the combined insights of retinex-based and deep learning-based approaches in low-light image enhancement. Retinex-based methods [12, 26, 45, 63] decompose the underwater image into reflectance and illumination components [21] and estimate the illumination to enhance the image quality. On the other hand, deep learning-based methods leverage techniques such as encoder-decoder networks [46, 59, 69, 70], bilateral learning [61], and adversarial learning [22, 72], to improve image quality.

In the following section, we present our method, which complements existing learning-based approaches by harnessing the strengths of modern deep neural networks while incorporating insights from an underlying physical model to enhance underwater images.

### 3. Methodology

Here, we present our two main components : (i) UIFM, which is used for backscatter estimation; (ii) PhISH-Net, the proposed deep image enhancement framework to enhance the backscatter-removed image.

#### 3.1. Underwater Image Formation Model

In this work, we employ the UIFM proposed in Sea-Thru [4]. According to this model, the formation of any image  $I$  captured underwater can be modeled using two components, the *direct signal* ( $D$ ) and *backscatter* ( $B$ ) [5]. For each channel  $c \in \{r, g, b\}$ , the image can be decomposed as

$$I_c = D_c + B_c \quad (1)$$

$D$  and  $B$  are governed by two coefficients, the *wideband* (RGB) *attenuation* ( $\beta_d$ ) and the *backscatter* coefficient ( $\beta_b$ ). Equation 1 is further expanded as follows:

$$I = J e^{-\beta_d z} + B^\infty (1 - e^{-\beta_b z}) \quad (2)$$

Here,  $J$  is the unattenuated scene that would have been captured if there was no water medium attenuating colors with depth  $z$ .  $B^\infty$  is the backscatter color. In this model, the coefficients  $\beta_d$  and  $\beta_b$  are considered to be distinct.  $\beta_b$  and  $\beta_d$  depend on several factors including object reflectance,

spectrum of ambient light, spectral response of the camera, the physical scattering and beam attenuation coefficients of the water body, all of which are functions of wavelength. Now, we describe the algorithm to estimate backscatter  $B$ , which is then used to obtain the direct signal  $D$  from the captured underwater image  $I$ .

#### 3.2. Backscatter Estimation

When light penetrates through the water surface and interacts with underwater objects, it undergoes scattering in various directions. Additionally, suspended particles in the water column contribute to the scattering phenomenon towards the surface, resulting in a form of noise known as backscatter. This is modelled as an additive signal, which degrades the quality of underwater images.

The amount of backscatter in an image increases exponentially with the depth  $z$  and eventually reaches saturation. In areas where the scene reflectance or illumination tends to zero, the captured image  $I \rightarrow B$ . Backscatter can hence be estimated by identifying such areas. Inspired by the dark channel prior, this is done by searching for the darkest RGB triplets based on the depth map. The depth map is first partitioned into 10 evenly spaced clusters. In each cluster, we search  $I$  for RGB triplets in the bottom 1%, the set of which we denote as  $\Omega$ . An overestimate of backscatter is  $\hat{B}(\Omega) \approx I(\Omega)$ , which can be modelled using Equation 2 as

$$\hat{B} = \underbrace{J' \cdot e^{-\beta_{d'} z}}_{\text{Residual term}} + B^\infty (1 - e^{-\beta_b z}) \quad (3)$$

Given an input image  $I$  and its corresponding depth map  $z$ , the coefficients  $B^\infty, \beta_b, \beta_{d'}$  and  $J'$  are estimated using a non-linear least squares fitting subject to bounds as described in [4]. This is summarized in Algorithm 1.

**Depth Estimation** To accurately estimate backscatter, an absolute depth map is required. While some datasets utilize structure-from-motion [4] with known objects for scale to obtain these depth maps, this approach is limited in datasets without pre-existing depth information. To overcome this challenge, we employ an off-the-shelf depth estimation network to generate depth maps. Specifically, we adopt a boosted version of monocular depth estimation proposed by [48], which builds upon MiDaS [37] without retraining the base model. This depth boosting framework enhances the depth map quality by iteratively incorporating scene structure information using double estimation and patch selection at different resolutions. We demonstrate the quality of depth images with and without boosting in the supplementary material. We further employ a heuristic to estimate the minimum and maximum depth values in the absence of explicit information.

---

**Algorithm 1** Backscatter Estimation

---

**Input:** Underwater image  $I$ , Depth map  $z$ .

- 1: **Initialization:**  $\Omega = \emptyset, D = 0$ .
- 2: Partition  $z$  in 10 evenly spaced clusters  $\Psi$  between  $\max(z)$  and  $\min(z)$ .
- 3: **for** cluster in  $\Psi$  **do**
- 4:   Add RGB triplets of  $I$  in the bottom 1% to  $\Omega$ .
- 5: **end for**
- 6: An overestimate of the backscatter is given by  $\hat{B}(\Omega) \approx I(\Omega)$ , which can be modelled using Eq.(2).
- 7: **for**  $c \in \{r, g, b\}$  **do**
- 8:   Estimate  $\hat{B}_c$  using a non-linear least squares fit on Eq.(3) and then obtain the direct signal.
- 9:    $D_c = I_c - \hat{B}_c$ .
- 10: **end for**

**Output:** Estimated backscatter  $\hat{B}$  and Direct signal  $D$ .

---

### 3.3. PhISH-Net

The direct signal estimated using the backscatter is often dimly lit. The task of enhancing this direct signal mimics the well explored low light image enhancement problem, which we draw inspiration from. At its core, image enhancement involves finding a mapping that enhances an input image  $I$  to produce an improved version  $\tilde{I}$ .

A well established image enhancement model is the retinex model, where an image captured  $I$  is composed of two components, Reflectance  $\tilde{I}$  and Illumination  $S$ . Mathematically, this is given as  $I = S * \tilde{I}$ , where  $*$  denotes a pixel-wise multiplication. In our case,  $I = D$ , the direct signal obtained after backscatter removal. As in several prior works [21, 26], we treat  $\tilde{I}$  as the enhanced image. Now, given  $I$ , the problem reduces to estimating the illumination map  $S$ , using which the enhanced image  $\tilde{I}$  can be obtained as  $S^{-1} * I$ . Although early works such as LIME [26] and DUAL [73] model  $S$  as a single-channel illumination map, recent studies [61] have shown that representing the illumination map using three channels yields better performance, especially in terms of colour enhancement and handling non-linearity across different colour channels.

In this work, we propose PhISH-Net to predict a three-channel illumination map  $S$ , which is then used to obtain the enhanced output image as  $\tilde{I} = I / (S + \epsilon)$ .

We propose to use a simple convolutional architecture equipped with a network designed to extract both global and local features, aiding in the estimation of bilateral grid coefficients [25]. These coefficients are then applied to the output of a *guide network*, to obtain a high-resolution illumination map  $S_{hr}$ . Subsequently, the enhanced image is computed as  $I_{out} = D_{hr} / (S_{hr} + \epsilon)$ . This allows most network computations to be performed at a reduced resolution, facilitating real-time processing of high-resolution

underwater images. This approach not only addresses computational efficiency but also enables the model to handle images of varying sizes. The overall pipeline for this image enhancement process is illustrated in Figure 2. We impose a novel prior on the wideband (RGB) attenuation coefficient  $\beta_d$  based on the experimental findings in [4]. PhISH-Net is optimized to predict the illumination map  $S_{hr}$  by minimizing the proposed attenuation loss, image reconstruction loss, color loss and smoothness loss. We first describe the proposed *wideband attenuation prior* and then describe each of the loss components.

**Wideband Attenuation Prior** The objective is to recover the unattenuated scene  $J$  from the estimated direct signal  $D$ , following the UIFM model described in Section 3.1. Considering the visual properties of the estimated direct signal mimic that of a low light image, the objective can alternatively be formulated based on retinex based image model to recover the reflectance component by estimating the illumination map. Sea-Thru draws inspiration from image-dehazing models, and [23] suggest that there is a linear relationship between image-dehazing and the retinex model. This in turn suggests that the objective of estimating the unattenuated scene  $J$  based on UIFM can be related to that of estimating reflectance based on Retinex model. Here, we propose a novel wideband attenuation prior through attenuation loss  $\mathcal{L}_a$ , which constrains the predicted output to follow both the image formation models. The attenuation component  $e^{-\beta_d z}$  being analogous to the illumination map  $S$ , we can obtain a coarse estimate of the wideband attenuation coefficient, given the depth map  $z$  and the predicted illumination map  $S_{hr}$  as follows.

$$\hat{\beta}_d(z) = \frac{-\log S_{hr}}{z} \quad (4)$$

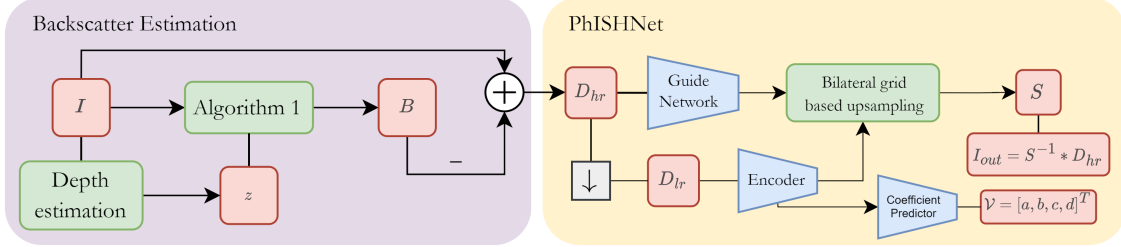
This coefficient is known to decay with depth  $z$  following a two-term exponential curve as shown below. This was established in [4] by performing extensive experimentation on a variety of underwater image datasets.

$$\beta_d(z) = a * e^{-b \cdot z} + c * e^{-d \cdot z} \quad (5)$$

PhISH-Net predicts the illumination map  $S_{hr}$  which we use to constrain the coarse estimate of the coefficient  $\beta_d$  obtained from Equation 4 to follow the curve in Equation 5 by using the following wideband attenuation prior loss  $\mathcal{L}_a$ .

$$\mathcal{L}_a = \|(-\frac{\log S_{hr}}{z}) - (a * e^{-b \cdot z} + c * e^{-d \cdot z})\|^2 \quad (6)$$

Here,  $a, b, c, d \in \mathbb{R}^+$  are obtained from a learnable coefficient predictor network using features extracted by the encoder block. We denote these coefficients by the vector  $\mathcal{V} = [a, b, c, d]$  in Figure 2.



$$\mathcal{L} = w_r \mathcal{L}_r(I_{out}, I_{gt}) + w_c \mathcal{L}_c(I_{out}, I_{gt}) + w_s \mathcal{L}_s(D_{hr}, S) + w_a \mathcal{L}_a(S, z, \mathcal{V})$$

Figure 2. Underwater Image Enhancement model: Here, we briefly illustrate the steps involved (1) *Backscatter Removal* (Section 3.2) (2) *PhISH-Net*: Given a high-resolution backscatter-removed image, we create a guide map and predict bilateral grid coefficients from its downsampled version. They are used to obtain a high-resolution illumination map, yielding the enhanced image via the retinex model.

**Reconstruction loss** is obtained as the  $L_2$  norm between the predicted enhanced image and the ground truth enhanced image  $I_{gt}$ . Here,  $c$  is the channel and  $c \in \{r, g, b\}$ .

$$\mathcal{L}_r = \|(\mathcal{S}_{hr}^{-1} * D_{hr}) - I_{gt}\|^2 \text{ s.t. } (D_{hr})_c \leq (\mathcal{S}_{hr})_c \leq 1 \quad (7)$$

**Color Loss** is employed to match the colors of the predicted output  $I_{out}$  with the ground truth image  $I_{gt}$ . This is achieved by minimizing the angle  $\angle(,)$  between each color pair for all pixels  $p$ . Here, each RGB color is considered as a vector in three dimensional space.

$$\mathcal{L}_c = \sum_p \angle((I_{out})_p, (I_{gt})_p) \quad (8)$$

**Smoothness Loss** is a weighted  $L_2$  norm of the gradients of the illumination map  $S$ . This is imposed based on the prior observation that illumination in natural images is typically locally smooth.

$$\mathcal{L}_s = \sum_p \sum_c \omega_{x,c}^p (\partial_x \mathcal{S}_p)_c^2 + \omega_{y,c}^p (\partial_y \mathcal{S}_p)_c^2 \quad (9)$$

The weights  $\omega_{x,c}^p$  and  $\omega_{y,c}^p$  are spatially varying smoothness weights designed to promote locally smooth variations on pixels with small gradients while allowing for discontinuous illumination on pixels with large gradients in the illumination map. In the context of underwater images, which are prone to inconsistent illumination, the smoothness loss helps mitigate the introduction of abrupt changes in the illumination map.

**Training PhISH-Net** Given an underwater image dataset  $D = \{(I^i, I_{gt}^i)\}_{i=1}^N$ , where  $I_{gt}^i$  is the enhanced version of the image  $I^i$  and  $N$  is the number of images, we train PhISH-Net using the following loss:

$$\mathcal{L}^i = w_r \mathcal{L}_r^i + w_c \mathcal{L}_c^i + w_s \mathcal{L}_s^i + w_a \mathcal{L}_a^i \quad (10)$$

where  $\mathcal{L}^i$  corresponds to the loss for the  $i^{th}$  image pair and  $w_r, w_c, w_s$  and  $w_a$  are the weights assigned to each loss component. The values are empirically set to  $w_r = 10, w_s = 2, w_c = 1$  and  $w_a = 0.5$ .

### 3.4. Photofinishing

Color correction is a crucial step in enhancing underwater images. To eliminate undesirable color casts, images are first white balanced, which improves their overall appearance. Previous work [8] has shown that artifacts are typically present in the red and blue channels, and are corrected.

$$\begin{aligned} I_{rc} &= I_r + \alpha_1 * (\bar{I}_g - \bar{I}_r) \\ I_{bc} &= I_b + \alpha_2 * (\bar{I}_g - \bar{I}_b) \end{aligned} \quad (11)$$

where  $I_{rc}$  and  $I_{bc}$  are the corrected red ( $I_r$ ) and blue ( $I_b$ ) channels respectively.  $\bar{I}_c$  denotes the mean value of channel  $c \in \{r, g, b\}$ . The combining coefficients  $\alpha_1$  and  $\alpha_2$  and are chosen between  $[0, 1]$ .

The final output is obtained through a multi-scale fusion technique based on a laplacian pyramid [11]. First, a gamma-corrected and unsharp masked version of the white-balanced image are generated to enhance global colour contrast and edge sharpness. The two versions are weighted using local image quality metrics such as the laplacian contrast weight, saliency weight, and saturation weight. The weights are chosen to preserve the desired qualities and reject undesired defaults of the inputs. The output of this step is convexly combined with the model’s output to allow for a more natural and visually appealing final image.

## 4. Experimental Results

**Datasets** In order to comprehensively assess the performance of our proposed approach, we conducted extensive experiments on two real-world underwater datasets: UIEB [40], EUVP [35]. The UIEB dataset consists of 890 underwater images with diverse scenes and varying levels of degradation. The EUVP dataset contains 5550 paired dark

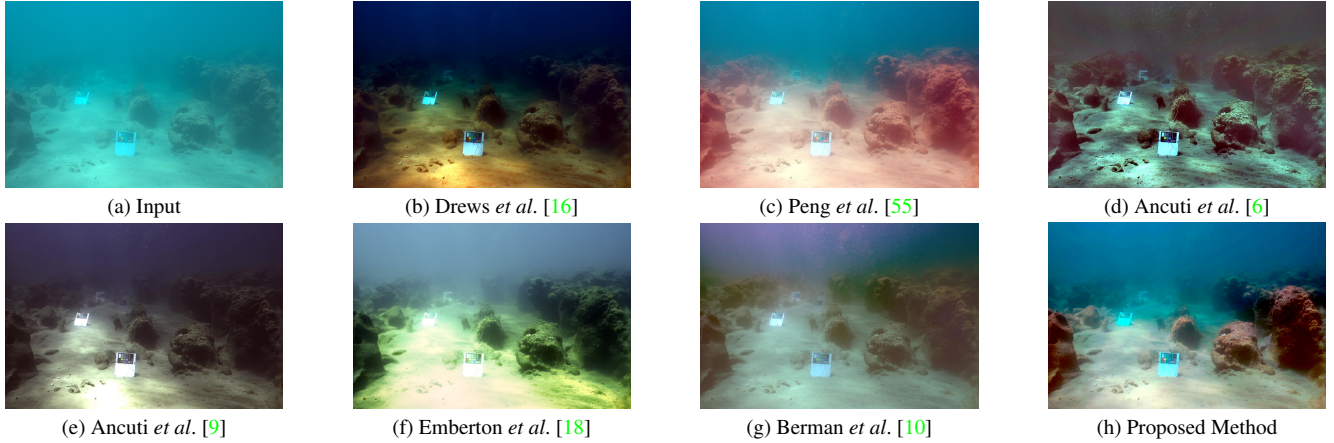


Figure 3. Results for various models on the sample *RGT\_3204* from the SQUID dataset.

images captured during oceanic explorations. We use 80:20 train-test split for these two datasets in all experiments. Further, we also use the SQUID [10] dataset which comprises 57 underwater images from different locations, representing various water properties and conditions. Due to the limited number of available images in SQUID dataset, here we evaluate the model trained on EUVP and qualitatively compare our method with prior approaches in Figure 3. This experiment also demonstrates the generalization ability of this method across datasets.

#### 4.1. Implementation Details

**Backscatter Estimation** We use an off-the-shelf depth boosting method [48] based on MiDaS [37], a monocular depth estimation method, without further retraining. The obtained depth map is used for backscatter estimation on the full-resolution underwater images.

**PhISH-Net** The model is built using PyTorch [51] and trained for 100 epochs with a batch size of 64 on an NVIDIA RTX A5000 GPU using the loss defined in Equation 10 and the Adam optimizer with a learning rate of  $1e-4$ . During training, the input images are resized to  $512 \times 512$  pixels, and a fixed size of  $256 \times 256$  pixels is used for the low-resolution input. An intermediate representation is obtained using a series of five convolutional blocks, which is then fed into the local and global feature extractor. The resulting local and global features are concatenated and upsampled using a bilateral grid-based module [25]. The architecture of each module is described in detail in the supplementary material. Given that the guide network is fully convolutional, it can handle images of any resolution at test time, enabling us to operate at the original resolution.

**Evaluation Metrics** To quantitatively evaluate the effectiveness of our proposed model, we employ a comprehensive set of both reference-based and non-reference-based quality metrics. The reference based metrics include Peak Signal-to-Noise Ratio (PSNR), PSNR for the Luminance channel (PSNR-L), Structural Similarity Index Measure (SSIM), and Patch-based Contrast Quality Index (PCQI) [62]. These metrics provide a comparative assessment by comparing the enhanced images with reference images. In addition, we also evaluate the model based on five non-reference-based metrics which evaluate the quality of enhanced images without relying on reference images. These include Underwater Colour Image Quality Evaluation (UCIQE) [71], Colorfulness Contrast Fog density index (CCF) [65], Underwater Image Quality Measure (UIQM), Underwater Image Colorfulness Measure (UICM) and Underwater Image Contrast Measure (UICOnM) [50]. It is important to note that higher values indicate better results and improved image quality for all these metrics.

**4.2. Additional Analysis**

In this section, we thoroughly evaluate and discuss the performance of the proposed framework. To provide a comprehensive assessment, we benchmark our approach against several existing UIE methods, enabling a comparative analysis. Moving beyond quantitative evaluations, we delve into qualitative results and present visual comparisons with previous methods, allowing for a deeper understanding of the improvements achieved. Furthermore, we conduct an ablation study to explore the individual contributions of each loss component in our framework. These discussions shed light on the importance of each component of our approach.

**Comparative Analysis** We present a thorough comparison of the proposed framework with various UIE methods on two datasets, UIEB and EUVP, including both traditional/model-based approaches [4, 14, 33, 54, 76] and deep learning-based methods [19, 30, 35, 36, 39, 60]. The

	Method	PSNR (↑)	PSNR <sub>L</sub> (↑)	SSIM (↑)	PCQI (↑)	UCIQE (↑)	UIQM (↑)	UICM (↑)	UIConM (↑)	CCF (↑)
UIEB	FUnIE-GAN [35]	17.3828	20.0596	0.7285	0.6393	0.5459	1.3993	5.7775	1.1605	21.0605
	UW-GAN [60]	16.2281	19.1524	0.7644	0.7187	0.5655	1.3467	5.5550	1.1219	22.8449
	UWCNN [39]	12.0247	13.7820	0.6469	0.3921	0.5058	1.0647	1.9216	0.9398	11.0019
	HLRP [76]	13.0317	13.7891	0.2874	0.2326	0.6356	<b>1.6477</b>	<b>9.5089</b>	<b>1.1915</b>	36.9312
	MLLE [74]	18.1079	19.4733	0.7985	0.9105	0.6044	1.6287	4.8271	1.0124	36.2740
	IBLA [54]	15.5610	17.7756	0.7390	0.6949	0.6020	1.4397	7.3312	1.0143	28.9752
	TOPAL [36]	20.5871	22.6706	0.8674	0.7148	0.5841	1.2209	5.0093	1.0321	21.2175
	UDCP [14]	11.9286	12.7288	0.6441	0.6117	0.5956	1.5725	7.1986	1.1748	27.1441
	Water-Net [40]	18.7003	19.7212	0.8623	0.6926	0.5711	1.2637	5.0644	1.0633	16.5005
	ICSP [33]	11.7942	13.1037	0.6340	0.7323	0.5636	1.4759	6.3012	1.0484	26.6930
PhISH-Net		<b>21.1390</b>	<b>23.4312</b>	<b>0.8686</b>	<b>0.9294</b>	<b>0.6405</b>	1.5968	8.8169	1.1513	<b>37.2389</b>
EUVP	FUnIE-GAN [35]	20.5600	27.4704	0.8866	0.8927	0.5086	1.5549	4.0977	1.2502	29.2321
	UW-GAN [60]	15.7630	22.8411	0.9155	0.9653	0.5262	1.4741	3.3911	1.2164	29.3064
	UWCNN [39]	15.5175	18.4511	0.8439	0.6451	0.5427	1.4212	1.6375	1.2607	19.5666
	HLRP [76]	12.4673	13.3926	0.2213	0.1722	0.5748	1.5591	4.0038	<b>1.2885</b>	30.0306
	MLLE [74]	14.2530	16.1892	0.6125	1.0295	0.5879	<b>1.7296</b>	2.9907	0.7756	36.2180
	IBLA [54]	16.9223	23.0862	0.8643	0.9891	0.5895	1.5616	4.6178	1.1100	39.5418
	TOPAL [36]	18.3044	24.4843	0.9335	0.9942	0.5826	1.4905	3.2523	1.1990	34.9025
	UDCP [14]	14.4190	18.2478	0.8140	0.8572	0.5908	1.6489	<b>4.7064</b>	1.1962	35.1508
	Water-Net [40]	18.2595	24.3506	<b>0.9357</b>	0.8831	0.5793	1.4975	3.1465	1.2309	25.6186
	ICSP [33]	12.1254	14.5056	0.6710	0.9797	0.5750	1.5896	4.0923	0.9728	<b>41.2878</b>
PhISH-Net		<b>20.9197</b>	<b>27.4717</b>	0.8559	<b>1.0378</b>	<b>0.5918</b>	1.5925	4.3570	1.1512	38.8619

Table 1. Image Quality Metrics of various UIE methods on the UIEB and EUVP datasets.

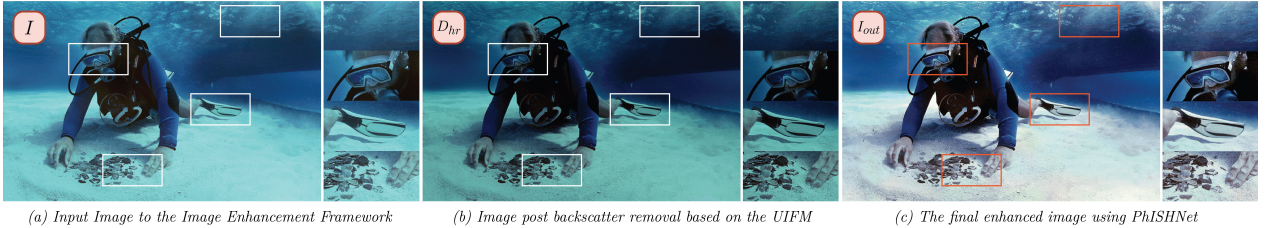


Figure 4. Stage-wise outputs of the proposed framework.

results, summarized in Table 1, clearly demonstrate the superiority of our approach over all previous methods on both datasets. While our model might not secure the highest ranking in certain non-reference-based metrics,

it's noteworthy to observe that techniques achieving high non-reference metrics tend to yield low reference-based metrics, particularly in terms of SSIM and PCQI. This topic has been elaborated upon in the supplementary material, alongside enhancements in metrics attributed to the photofinishing step. Additionally, stage-wise results are shown in Figure 4. Overall, these quantitative evaluations establish the superiority of our proposed framework over previous works.

**Qualitative results** We further demonstrate the effectiveness of our framework by showcasing sample results from two datasets: UIEB and EUVP (see Figures 1 and 6 respectively). Additionally, we evaluate the generalization

$\mathcal{L}_r$	$\mathcal{L}_c$	$\mathcal{L}_s$	$\mathcal{L}_a$	PSNR (↑)	SSIM (↑)
✓				20.7987	0.8299
✓	✓			20.8560	0.8319
✓	✓	✓		20.8671	0.8320
✓	✓	✓	✓	21.1390	0.8686

Table 2. Ablation study of loss components on UIEB dataset

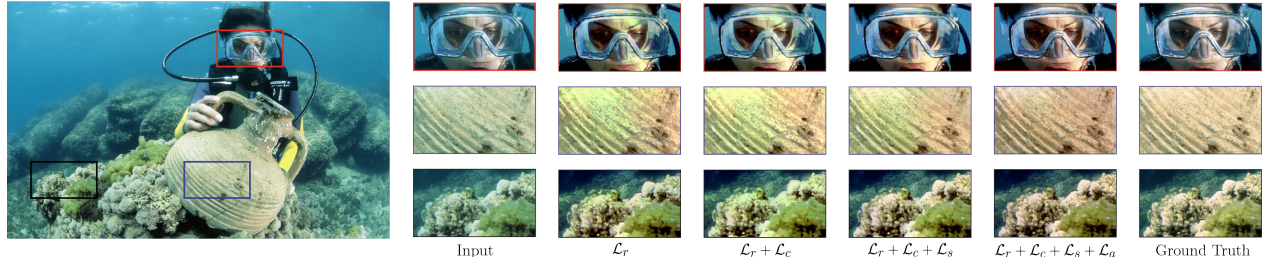


Figure 5. Results of the ablation study that demonstrates the effectiveness of each component in the loss function.

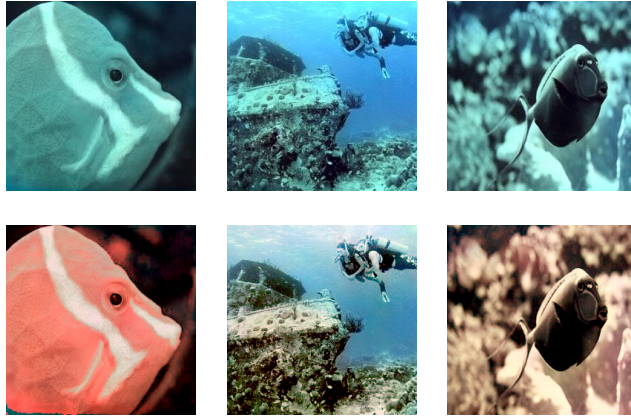


Figure 6. Sample results for images from the EUVP dataset. **Top:** input; **Bottom:** corresponding model output.

capability of PhISH-Net through a cross-dataset scenario. Specifically, we test SQUID images on the EUVP trained model and present the results in Figure 3. We also investigate the utility of enhanced images for downstream tasks by analyzing SIFT features, which we demonstrate in the supplementary material.

#### Ablation Study

To assess the significance of each loss

Method	Runtime (s) ( $\downarrow$ )			GFLOPs ( $\downarrow$ )	Parameters ( $\downarrow$ )
	256x256	512x512	1024x1024		
Sea-Thru	[4]	2.84940	10.5835	43.9366	-
UDCP	[14]	2.09800	5.02730	12.2055	-
ICSP	[33]	0.56110	2.31270	4.66480	-
HLRP	[76]	1.45400	1.62400	2.09600	-
IBLA	[54]	3.34579	14.0217	57.0798	-
UGAN	[19]	0.00131	-	18.1547	54.4041
FUNIE-GAN	[35]	0.00122	-	10.2388	7.01959
FE-GAN	[30]	-	-	2.84000	11.4760
UW-GAN	[60]	0.00037	-	0.00385	1.92567
UWCNN	[39]	0.21299	0.44511	2.14731	28.4671
TOPAL	[36]	0.50230	1.98956	8.33497	111.6193
Water-Net	[40]	1.03550	2.54530	4.62990	142.9039
PhISH-Net (network)		0.00216	0.00280	0.00413	-
PhISH-Net (pre/post)		0.21160	0.46964	1.66681	-
PhISH-Net (overall)		0.21376	0.47244	1.67095	0.09001
					0.55620

Table 3. Complexity Analysis of PhISH-Net.

component in our proposed approach, we conducted a comprehensive ablation study. The results, presented in Figure 5, highlight the consistent improvement in model performance with the addition of each loss term. Additionally, we analyze the impact of each extra component on quality metrics, as summarized in Table 2. We observe the PSNR and SSIM metrics improve significantly as each individual loss term is incorporated, indicating superior image quality. Overall, the ablation study provides valuable insights into the efficacy of our proposed loss. Additionally, we conducted ablation studies by altering the intrinsic parameters of the model and evaluating its robustness against image and depth degradations. Further details are provided in the supplementary material.

**Complexity Analysis** We evaluate our method’s complexity in FLOPs, parameters, and runtime (Table 3). We observe that our model achieves a significant improvement in run-time, even for high-resolution underwater images. In terms of parameters and FLOPs, the proposed model is extremely lightweight, at only 0.55M parameters.

## 5. Conclusion

In this paper, we have presented an effective framework for underwater image enhancement that combines a physics-based UIFM with a deep image enhancement approach based on the retinex model. Our proposed PhISH-Net framework achieves real-time processing of high-resolution underwater images using a lightweight neural network and a bilateral-grid-based upsampler. By introducing a novel *Wideband Attenuation prior*, we account for the optical characteristics and color attenuation properties of water while also following the retinex model. Extensive experiments on two underwater image datasets demonstrate the superior performance of our method compared to state-of-the-art techniques. Additionally, our approach showcases cross-dataset generalization capability. Overall, our contributions lie in the integration of physics-based modeling, deep image enhancement, and efficient processing, offering a compelling solution for the underwater image enhancement task.

## References

- [1] Ahmad Shahrizan Abdul Ghani and Nor Ashidi Mat Isa. Underwater image quality enhancement through composition of dual-intensity images and rayleigh-stretching. *SpringerPlus*, 3(1):757, Dec 2014. 1
- [2] Ahmad Shahrizan Abdul Ghani and Nor Ashidi Mat Isa. Underwater image quality enhancement through integrated color model with rayleigh distribution. *Applied Soft Computing*, 27:219–230, 2015. 1
- [3] Derya Akkaynak and Tali Treibitz. A revised underwater image formation model. In *IEEE/CVF Conference on Computer Vision and Pattern Recognition*, pages 6723–6732, 2018. 1, 2
- [4] Derya Akkaynak and Tali Treibitz. Sea-thru: A method for removing water from underwater images. In *IEEE/CVF Conference on Computer Vision and Pattern Recognition*, pages 1682–1691, 2019. 1, 2, 3, 4, 6, 8
- [5] Derya Akkaynak, Tali Treibitz, Tom Shlesinger, Yossi Loya, Raz Tamir, and David Iluz. What is the space of attenuation coefficients in underwater computer vision? In *IEEE Conference on Computer Vision and Pattern Recognition*, pages 568–577, 2017. 3
- [6] Cosmin Ancuti, Codruta O. Ancuti, Christophe De Vleeschouwer, Rafael Garcia, and Alan C. Bovik. Multi-scale underwater descattering. In *International Conference on Pattern Recognition*, pages 4202–4207, 2016. 6
- [7] Cosmin Ancuti, Codruta Orniana Ancuti, Tom Haber, and Philippe Bekaert. Enhancing underwater images and videos by fusion. In *2012 IEEE Conference on Computer Vision and Pattern Recognition*, pages 81–88, 2012. 2
- [8] Codruta O. Ancuti, Cosmin Ancuti, Christophe De Vleeschouwer, and Philippe Bekaert. Color balance and fusion for underwater image enhancement. *IEEE Transactions on Image Processing*, 27(1):379–393, 2018. 2, 5
- [9] Codruta O. Ancuti, Cosmin Ancuti, Christophe De Vleeschouwer, Laszlo Neumann, and Rafael Garcia. Color transfer for underwater dehazing and depth estimation. In *IEEE International Conference on Image Processing*, pages 695–699, 2017. 6
- [10] D. Berman, D. Levy, S. Avidan, and T. Treibitz. Underwater single image color restoration using haze-lines and a new quantitative dataset. *IEEE Transactions on Pattern Analysis & Machine Intelligence*, 43(08):2822–2837, 2021. 1, 2, 6
- [11] P. Burt and E. Adelson. The laplacian pyramid as a compact image code. *IEEE Transactions on Communications*, 31(4):532–540, 1983. 5
- [12] Bolun Cai, Xianming Xu, Kailing Guo, Kui Jia, Bin Hu, and Dacheng Tao. A joint intrinsic-extrinsic prior model for retinex. In *IEEE International Conference on Computer Vision*, pages 4020–4029, 2017. 3
- [13] Paulo L.J. Drews, Erickson R. Nascimento, Silvia S.C. Botelho, and Mario Fernando Montenegro Campos. Underwater depth estimation and image restoration based on single images. *IEEE Computer Graphics and Applications*, 36(2):24–35, 2016. 2
- [14] Paulo L.J. Drews, Erickson R. Nascimento, Silvia S.C. Botelho, and Mario Fernando Montenegro Campos. Underwater depth estimation and image restoration based on single images. *IEEE Computer Graphics and Applications*, 36(2):24–35, 2016. 2, 6, 7, 8
- [15] P. Drews Jr, E. do Nascimento, F. Moraes, S. Botelho, and M. Campos. Transmission estimation in underwater single images. In *IEEE International Conference on Computer Vision Workshops*, pages 825–830, 2013. 2
- [16] Paulo L. J. Drews-Jr, Erickson R. Nascimento, Felipe Codevilla Moraes, Silvia S. C. Botelho, and Mario Fernando Montenegro Campos. Transmission estimation in underwater single images. *2013 IEEE International Conference on Computer Vision Workshops*, pages 825–830, 2013. 6
- [17] Akshay Dudhane, Praful Hambarde, Prashant Patil, and Subrahmanyam Murala. Deep underwater image restoration and beyond. *IEEE Signal Processing Letters*, 27:675–679, 2020. 1
- [18] Simon Emberton, Lars Chittka, and Andrea Cavallaro. Underwater image and video dehazing with pure haze region segmentation. *Computer Vision and Image Understanding*, 168:145–156, 2018. Special Issue on Vision and Computational Photography and Graphics. 6
- [19] Cameron Fabbri, Md Jahidul Islam, and Junaid Sattar. Enhancing underwater imagery using generative adversarial networks. In *IEEE International Conference on Robotics and Automation*, pages 7159–7165, 2018. 3, 6, 8
- [20] Xueyang Fu and Xiangyong Cao. Underwater image enhancement with global-local networks and compressed-histogram equalization. *Signal Processing: Image Communication*, 86:115892, 2020. 1
- [21] Xueyang Fu, Delu Zeng, Yue Huang, Xiao-Ping Zhang, and Xinghao Ding. A weighted variational model for simultaneous reflectance and illumination estimation. In *IEEE Conference on Computer Vision and Pattern Recognition*, pages 2782–2790, 2016. 3, 4
- [22] Ying Fu, Yang Hong, Linwei Chen, and Shaodi You. Le-gan: Unsupervised low-light image enhancement network using attention module and identity invariant loss. *Knowledge-Based Systems*, 240:108010, 2022. 3
- [23] Adrian Galdran, Alessandro Bria, Aitor Alvarez-Gila, Javier Vazquez-Corral, and Marcelo Bertalmio. On the duality between retinex and image dehazing. In *IEEE/CVF Conference on Computer Vision and Pattern Recognition*, pages 8212–8221, 2018. 4
- [24] Adrian Galdran, David Pardo, Artzai Picón, and Aitor Alvarez-Gila. Automatic red-channel underwater image restoration. *Journal of Visual Communication and Image Representation*, 26:132–145, 2015. 2
- [25] Michaël Gharbi, Jiawen Chen, Jonathan T Barron, Samuel W Hasinoff, and Frédéric Durand. Deep bilateral learning for real-time image enhancement. *ACM Transactions on Graphics*, 36(4):118, 2017. 4, 6
- [26] Xiaojie Guo, Yu Li, and Haibin Ling. Lime: Low-light image enhancement via illumination map estimation. *IEEE Transactions on Image Processing*, 26(2):982–993, 2017. 3, 4

- [27] Yecai Guo, Hanyu Li, and Peixian Zhuang. Underwater image enhancement using a multiscale dense generative adversarial network. *IEEE Journal of Oceanic Engineering*, 45(3):862–870, 2020. 3
- [28] Gür Emre Güraksin, Utku Köse, and Ömer Deperlioğlu. Underwater image enhancement based on contrast adjustment via differential evolution algorithm. In *2016 International Symposium on INnovations in Intelligent SysTems and Applications (INISTA)*, pages 1–5, 2016. 1
- [29] Jie Han, Jian Zhou, Lin Wang, Yu Wang, and Zhongjun Ding. Fe-gan: Fast and efficient underwater image enhancement model based on conditional gan. *Electronics*, 12(5):1227, Mar 2023. 3
- [30] Jie Han, Jian Zhou, Lin Wang, Yu Wang, and Zhongjun Ding. Fe-gan: Fast and efficient underwater image enhancement model based on conditional gan. *Electronics*, 12(5), 2023. 6, 8
- [31] Ruyue Han, Yang Guan, Zhibin Yu, Peng Liu, and Haiyong Zheng. Underwater image enhancement based on a spiral generative adversarial framework. *IEEE Access*, 8:218838–218852, 2020. 3
- [32] Najmul Hassan, Sami Ullah, Naeem Bhatti, Hasan Mahmood, and Muhammad Zia. The retinex based improved underwater image enhancement. *Multimedia Tools and Applications*, 80(2):1839–1857, Jan 2021. 2
- [33] Guojia Hou, Nan Li, Peixian Zhuang, Kunqian Li, Haihan Sun, and Chongyi Li. Non-uniform illumination underwater image restoration via illumination channel sparsity prior. *IEEE Transactions on Circuits and Systems for Video Technology*, pages 1–1, 2023. 2, 6, 7, 8
- [34] Kashif Iqbal, Michael Odetayo, Anne James, Rosalina Abdul Salam, and Abdullah Zawawi Hj Talib. Enhancing the low quality images using unsupervised colour correction method. In *2010 IEEE International Conference on Systems, Man and Cybernetics*, pages 1703–1709, 2010. 2
- [35] Md Jahidul Islam, Youya Xia, and Junaed Sattar. Fast underwater image enhancement for improved visual perception. *IEEE Robotics and Automation Letters*, 5(2):3227–3234, 2020. 1, 2, 3, 5, 6, 7, 8
- [36] Zhiying Jiang, Zhuoxiao Li, Shuzhou Yang, Xin Fan, and Risheng Liu. Target oriented perceptual adversarial fusion network for underwater image enhancement. *IEEE Transactions on Circuits and Systems for Video Technology*, 32(10):6584–6598, 2022. 3, 6, 7, 8
- [37] Katrin Lasinger, René Ranftl, Konrad Schindler, and Vladlen Koltun. Towards robust monocular depth estimation: Mixing datasets for zero-shot cross-dataset transfer. *CoRR*, abs/1907.01341, 2019. 3, 6
- [38] Chongyi Li, Saeed Anwar, and Fatih Porikli. Underwater scene prior inspired deep underwater image and video enhancement. *Pattern Recognition*, 98:107038, 2020. 2
- [39] Chongyi Li, Saeed Anwar, and Fatih Porikli. Underwater scene prior inspired deep underwater image and video enhancement. *Pattern Recognition*, 98:107038, 2020. 6, 7, 8
- [40] Chongyi Li, Chunle Guo, Wenqi Ren, Runmin Cong, Junhui Hou, Sam Kwong, and Dacheng Tao. An underwater image enhancement benchmark dataset and beyond. *IEEE Trans-* actions on Image Processing, 29:4376–4389, 2020. 1, 2, 5, 7, 8
- [41] Chongyi Li, Jichang Guo, and Chunle Guo. Emerging from water: Underwater image color correction based on weakly supervised color transfer. *IEEE Signal Processing Letters*, 25(3):323–327, 2018. 3
- [42] Chong-Yi Li, Ji-Chang Guo, Run-Min Cong, Yan-Wei Pang, and Bo Wang. Underwater image enhancement by dehazing with minimum information loss and histogram distribution prior. *IEEE Transactions on Image Processing*, 25(12):5664–5677, 2016. 2
- [43] Jie Li, Katherine A. Skinner, Ryan M. Eustice, and Matthew Johnson-Roberson. Watergan: Unsupervised generative network to enable real-time color correction of monocular underwater images. *CoRR*, abs/1702.07392, 2017. 1
- [44] Jie Li, Katherine A. Skinner, Ryan M. Eustice, and Matthew Johnson-Roberson. Watergan: Unsupervised generative network to enable real-time color correction of monocular underwater images. *IEEE Robotics and Automation Letters*, 3(1):387–394, 2018. 3
- [45] R. Liu, L. Ma, J. Zhang, X. Fan, and Z. Luo. Retinex-inspired unrolling with cooperative prior architecture search for low-light image enhancement. In *IEEE/CVF Conference on Computer Vision and Pattern Recognition*, pages 10556–10565, 2021. 3
- [46] Kin Gwn Lore, Adedotun Akintayo, and Soumik Sarkar. LInet: A deep autoencoder approach to natural low-light image enhancement. *Pattern Recognition*, 61:650–662, 2017. 3
- [47] Monika Mathur and Nidhi Goel. Enhancement of underwater images using white balancing and rayleigh-stretching. In *International Conference on Signal Processing and Integrated Networks*, pages 924–929, 2018. 2
- [48] S. Mahdi H. Miangoleh, Sebastian Dille, Long Mai, Sylvain Paris, and Yağız Aksoy. Boosting monocular depth estimation models to high-resolution via content-adaptive multi-resolution merging. In *IEEE/CVF Conference on Computer Vision and Pattern Recognition*, pages 9680–9689, 2021. 2, 3, 6
- [49] Sangeetha Mohan and Philomina Simon. Underwater image enhancement based on histogram manipulation and multiscale fusion. *Procedia Computer Science*, 171:941–950, 2020. International Conference on Computing and Network Communications (CoCoNet'19). 2
- [50] Karen Panetta, Chen Gao, and Sos Agaian. Human-visual-system-inspired underwater image quality measures. *IEEE Journal of Oceanic Engineering*, 41(3):541–551, 2016. 6
- [51] Adam Paszke, Sam Gross, Francisco Massa, Adam Lerer, James Bradbury, Gregory Chanan, Trevor Killeen, Zeming Lin, Natalia Gimelshein, Luca Antiga, Alban Desmaison, Andreas Köpf, Edward Z. Yang, Zach DeVito, Martin Raison, Alykhan Tejani, Sasank Chilamkurthy, Benoit Steiner, Lu Fang, Junjie Bai, and Soumith Chintala. Pytorch: An imperative style, high-performance deep learning library. *CoRR*, abs/1912.01703, 2019. 6
- [52] Soo-Chang Pei and Chia-Yi Chen. Underwater images enhancement by revised underwater images formation model. *IEEE Access*, 10:108817–108831, 2022. 1, 2

- [53] Yan-Tsung Peng, Keming Cao, and Pamela C. Cosman. Generalization of the dark channel prior for single image restoration. *IEEE Transactions on Image Processing*, 27(6):2856–2868, 2018. 2
- [54] Yan-Tsung Peng and Pamela C. Cosman. Underwater image restoration based on image blurriness and light absorption. *IEEE Transactions on Image Processing*, 26(4):1579–1594, 2017. 6, 7, 8
- [55] Yan-Tsung Peng, Xiangyun Zhao, and Pamela C. Cosman. Single underwater image enhancement using depth estimation based on blurriness. In *IEEE International Conference on Image Processing*, pages 4952–4956, 2015. 6
- [56] Qi Qi, Kunqian Li, Haiyong Zheng, Xiang Gao, Guojia Hou, and Kun Sun. Sguie-net: Semantic attention guided underwater image enhancement with multi-scale perception. *IEEE Transactions on Image Processing*, 31:6816–6830, 2022. 2
- [57] Qi Qi, Yongchang Zhang, Fei Tian, Q. M. Jonathan Wu, Kunqian Li, Xin Luan, and Dalei Song. Underwater image co-enhancement with correlation feature matching and joint learning. *IEEE Transactions on Circuits and Systems for Video Technology*, 32(3):1133–1147, 2022. 3
- [58] Yosuke Ueki and Masaaki Ikehara. Weighted generalization of dark channel prior with adaptive color correction for defogging. In *European Signal Processing Conference*, pages 685–689, 2021. 2
- [59] Haoyuan Wang, Ke Xu, and Rynson W. H. Lau. Local color distributions prior for image enhancement. In *Proceedings of the European Conference on Computer Vision*, 2022. 3
- [60] Nan Wang, Yabin Zhou, Fenglei Han, Haitao Zhu, and Jingzheng Yao. Uwgan: Underwater gan for real-world underwater color restoration and dehazing, 2019. 3, 6, 7, 8
- [61] Ruixing Wang, Qing Zhang, Chi-Wing Fu, Xiaoyong Shen, Wei-Shi Zheng, and Jiaya Jia. Underexposed photo enhancement using deep illumination estimation. In *IEEE/CVF Conference on Computer Vision and Pattern Recognition*, pages 6842–6850, 2019. 3, 4
- [62] Shiqi Wang, Kede Ma, Hojatollah Yeganeh, Zhou Wang, and Weisi Lin. A patch-structure representation method for quality assessment of contrast changed images. *IEEE Signal Processing Letters*, 22(12):2387–2390, 2015. 6
- [63] Shuhang Wang, Jin Zheng, Hai-Miao Hu, and Bo Li. Naturalness preserved enhancement algorithm for non-uniform illumination images. *IEEE Transactions on Image Processing*, 22(9):3538–3548, 2013. 3
- [64] Yang Wang, Yang Cao, Jing Zhang, Feng Wu, and Zheng-Jun Zha. Leveraging deep statistics for underwater image enhancement. *ACM Trans. Multimedia Comput. Commun. Appl.*, 17(3s), oct 2021. 3
- [65] Yan Wang, Na Li, Zongying Li, Zhaorui Gu, Haiyong Zheng, Bing Zheng, and Mengnan Sun. An imaging-inspired no-reference underwater color image quality assessment metric. *Computers & Electrical Engineering*, 70:904–913, 2018. 6
- [66] Yi Wang, Hui Liu, and Lap-Pui Chau. Single underwater image restoration using adaptive attenuation-curve prior. *IEEE Transactions on Circuits and Systems I: Regular Papers*, 65(3):992–1002, 2018. 2
- [67] Zhengyong Wang, Liquan Shen, Mai Xu, Mei Yu, Kun Wang, and Yufei Lin. Domain adaptation for underwater image enhancement. *IEEE Transactions on Image Processing*, 32:1442–1457, 2023. 3
- [68] Jun Xie, Guojia Hou, Guodong Wang, and Zhenkuan Pan. A variational framework for underwater image dehazing and deblurring. *IEEE Transactions on Circuits and Systems for Video Technology*, 32(6):3514–3526, 2022. 2
- [69] Ke Xu, Xin Yang, Baocai Yin, and Rynson W.H. Lau. Learning to restore low-light images via decomposition-and-enhancement. In *IEEE/CVF Conference on Computer Vision and Pattern Recognition*, pages 2278–2287, 2020. 3
- [70] Xiaogang Xu, Ruixing Wang, Chi-Wing Fu, and Jiaya Jia. Snr-aware low-light image enhancement. In *IEEE/CVF Conference on Computer Vision and Pattern Recognition*, pages 17693–17703, 2022. 3
- [71] Miao Yang and Arcot Sowmya. An underwater color image quality evaluation metric. *IEEE Transactions on Image Processing*, 24(12):6062–6071, 2015. 6
- [72] Wenhan Yang, Shiqi Wang, Yuming Fang, Yue Wang, and Jiaying Liu. From fidelity to perceptual quality: A semi-supervised approach for low-light image enhancement. In *IEEE/CVF Conference on Computer Vision and Pattern Recognition*, pages 3060–3069, 2020. 3
- [73] Qing Zhang, Yongwei Nie, and Wei-Shi Zheng. Dual illumination estimation for robust exposure correction, 2019. 4
- [74] Weidong Zhang, Peixian Zhuang, Hai-Han Sun, Guohou Li, Sam Kwong, and Chongyi Li. Underwater image enhancement via minimal color loss and locally adaptive contrast enhancement. *IEEE Transactions on Image Processing*, 31:3997–4010, 2022. 2, 7
- [75] Jingchun Zhou, Tongyu Yang, Weishen Chu, and Weishi Zhang. Underwater image restoration via backscatter pixel prior and color compensation. *Engineering Applications of Artificial Intelligence*, 111:104785, 2022. 2
- [76] Peixian Zhuang, Jiamin Wu, Fatih Porikli, and Chongyi Li. Underwater image enhancement with hyper-laplacian reflectance priors. *IEEE Transactions on Image Processing*, 31:5442–5455, 2022. 2, 6, 7, 8